

ARTICLES

Two stellar components in the halo of the Milky Way

Daniela Carollo^{1,2,3,5}, Timothy C. Beers^{2,3}, Young Sun Lee^{2,3}, Masashi Chiba⁴, John E. Norris⁵, Ronald Wilhelm⁶, Thirupathi Sivarani^{2,3}, Brian Marsteller^{2,3}, Jeffrey A. Munn⁷, Coryn A. L. Bailer-Jones⁸, Paola Re Fiorentin^{8,9} & Donald G. York^{10,11}

The halo of the Milky Way provides unique elemental abundance and kinematic information on the first objects to form in the Universe, and this information can be used to tightly constrain models of galaxy formation and evolution. Although the halo was once considered a single component, evidence for its dichotomy has slowly emerged in recent years from inspection of small samples of halo objects. Here we show that the halo is indeed clearly divisible into two broadly overlapping structural components—an inner and an outer halo—that exhibit different spatial density profiles, stellar orbits and stellar metallicities (abundances of elements heavier than helium). The inner halo has a modest net prograde rotation, whereas the outer halo exhibits a net retrograde rotation and a peak metallicity one-third that of the inner halo. These properties indicate that the individual halo components probably formed in fundamentally different ways, through successive dissipational (inner) and dissipationless (outer) mergers and tidal disruption of proto-Galactic clumps.

Astronomers have long sought to constrain models for the formation and evolution of the Milky Way (our Galaxy) on the basis of observations of the stellar and globular cluster populations that it contains. These populations are traditionally defined as samples of objects that exhibit common spatial distributions, kinematics and metallicities (the age of a population, when available, is also sometimes used). Metallicity is taken by astronomers to represent the abundances of elements heavier than helium, which are only created by nucleosynthesis in stars—either internally via nuclear burning in their cores or externally during explosive nucleosynthesis at the end of their lives. The earliest generations of stars have the lowest metallicities, because the gas from which they formed had not been enriched in heavy elements created by previous stars and distributed throughout the primordial interstellar medium by stellar winds and supernovae.

Previous work has provided evidence that the halo of the Milky Way may not comprise a single population, primarily from analysis of the spatial profiles (or inferred spatial profiles) of halo objects^{1–4}. A recent example of such an analysis is the observation of two different spatial density profiles for distinct classes of RR Lyrae variable stars in the halo⁵. In addition, tentative claims for a net retrograde motion of halo objects by previous authors supports the existence of a likely dual-component halo^{6–10}. The central difficulty in establishing with confidence whether or not a dichotomy of the halo populations exists is that the past samples of tracer objects have been quite small, and usually suitable only for consideration of a limited number of the expected signatures of its presence.

In the present work, we examine this question in detail using a large, homogeneously selected and analysed sample of over 20,000 stars, originally obtained as calibration data during the course of the Sloan Digital Sky Survey (SDSS)¹¹. Although there are many possible alternative (and more complex) models that might be considered,

multiple lines of evidence derived from these data clearly confirm that the halo can be resolved into (at least) two primary populations, the inner and the outer halo, with very different observed properties.

We find that the inner-halo component of the Milky Way dominates the population of halo stars found at distances up to 10–15 kpc from the Galactic Centre (including the solar neighbourhood). An outer-halo component dominates in the regions beyond 15–20 kpc. We show the inner halo to be a population of stars that are non-spherically distributed about the centre of the Galaxy, with an inferred axial ratio of the order of ~ 0.6 . Inner-halo stars possess generally high orbital eccentricities, and exhibit a modest prograde rotation (between 0 and 50 km s⁻¹) around the centre of the Galaxy (see Supplementary Table 1). The distribution of metallicities for stars in the inner halo peaks at $[\text{Fe}/\text{H}] \approx 2.1.6$, with tails extending to higher and lower metallicities. (Here metallicity is defined as $[A/B] \approx \log_{10}(N_A/N_B) - \log_{10}(N_A/N_B)_\odot$, where N_A and N_B represent the number density of atoms of elements A and B, and the subscript \odot indicates solar values.) The outer halo, by contrast, comprises stars that exhibit a much more spherical spatial distribution, with an axial ratio of ~ 0.9 – 1.0 . Outer-halo stars cover a wide range of orbital eccentricities, including many with lower eccentricity orbits than found for most stars associated with the inner halo, and exhibit a clear retrograde net rotation (between -40 and -70 km s⁻¹) about the centre of the Galaxy. The metallicity distribution function (MDF) of the outer halo peaks at lower metallicity than that of the inner halo, around $[\text{Fe}/\text{H}] \approx 2.2.2$, and includes a larger fraction of low-metallicity stars than does the MDF of the inner-halo population.

Evidence for the dichotomy of the halo

The spectroscopy, photometry and astrometry for our large sample of stars were obtained from observations carried out with the Apache Point 2.5-m SDSS telescope; these data are publicly available as Data

¹INAF—Osservatorio Astronomico di Torino, 10025 Pino Torinese, Italy. ²Department of Physics and Astronomy, Center for the Study of Cosmic Evolution, ³Joint Institute for Nuclear Astrophysics, Michigan State University, E. Lansing, Michigan 48824, USA. ⁴Astronomical Institute, Tohoku University, Sendai 980-8578, Japan. ⁵Research School of Astronomy and Astrophysics, The Australian National University, Mount Stromlo Observatory, Cotter Road, Weston, Australian Capital Territory 2611, Australia. ⁶Department of Physics, Texas Tech University, Lubbock, Texas 79409, USA. ⁷US Naval Observatory, PO Box 1149, Flagstaff, Arizona 86002, USA. ⁸Max-Planck-Institut für Astronomie, Königstuhl 17, D-69117, Heidelberg, Germany. ⁹Department of Physics, University of Ljubljana, Jadranska 19, 1000, Ljubljana, Slovenia. ¹⁰Department of Astronomy and Astrophysics, ¹¹The Enrico Fermi Institute, University of Chicago, Chicago, Illinois 60637, USA.

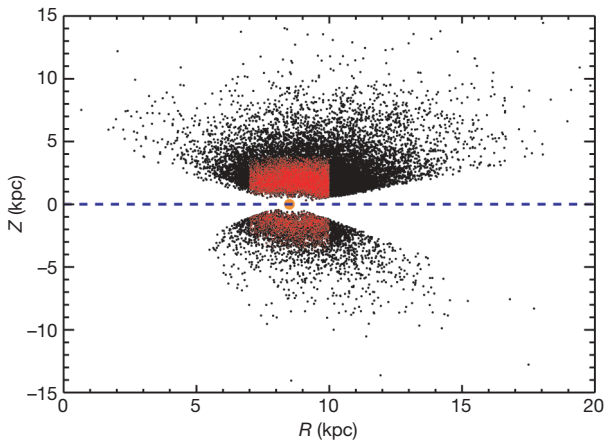


Figure 1 | The spatial distribution of the stars analysed in the present sample. The distribution of the full sample of 20,236 unique SDSS (Data Release 5¹²) spectrophotometric and telluric calibration stars in the Z - R plane is shown, where Z is the derived distance from the Galactic plane in the vertical direction and R is the derived distance from the centre of the Galaxy projected onto this plane. The dashed blue line represents the Galactic plane, while the filled orange dot is the position of the Sun, at $Z \approx 0$ kpc and $R \approx 8.5$ kpc. The ‘wedge shape’ of the selection area is the result of limits of the SDSS footprint in Galactic latitude. The red points indicate the 10,123 stars that satisfy our criteria for a local sample of stars, having $Z \lesssim 7$ kpc, $R \approx 10$ kpc, with distance estimates from the Sun $d \lesssim 4$ kpc, and with viable measurements of stellar parameters and proper motions.

Release 5¹². Details concerning the selection of the stars and the measurement of their parameters (temperature, surface gravity and metallicity, $[\text{Fe}/\text{H}]$), as well as the methods used to obtain their

estimated distances, proper motions and derived kinematics, can be found in the Supplementary Information.

Our 20,236 programme stars explore distances up to 20 kpc from the Sun, but we can only obtain useful estimates of the full space motions (as described in the Supplementary Information) for the subset of 10,123 stars in a local volume (up to 4 kpc from the Sun; Fig. 1). The restriction of the sample to the region of the solar neighbourhood is also made so that the assumptions going into the kinematic calculations are best satisfied. Figure 2 shows the distribution of $[\text{Fe}/\text{H}]$ for different cuts in the V velocity, which is the orbital component that measures the motion of a star (with respect to the Local Standard of Rest) in the rotation direction of the Galaxy. The transition in the distribution of $[\text{Fe}/\text{H}]$ that is expected as one sweeps from stars with thick-disk-like motions to stars with halo-like motions is clear. However, with the large sample of stars in our sample, it is possible to investigate the change in the distribution of $[\text{Fe}/\text{H}]$ for stars that are increasingly more retrograde, as well as for those that are both highly retrograde and have orbits taking them to high Z_{max} (the maximum distance above the Galactic plane reached by a star during the course of its orbit about the Galactic Centre—the Supplementary Information describes the methods used to derive this fundamental parameter). This figure shows that stars with the most retrograde orbits, and those that reach large distances in their orbits above the Galactic plane, exhibit distributions of $[\text{Fe}/\text{H}]$ that peak at metallicities between ≈ 2.0 and ≈ 2.2 , which we associate with the outer-halo population. The inner-halo population dominates the samples of stars with peak metallicity $[\text{Fe}/\text{H}] \approx 2.1.6$.

Astronomers have long debated whether there might exist a change in the rotational properties of the halo of the Milky Way as a function of distance from the Galactic Centre, based on much smaller samples of globular clusters^{2,10} and stars^{6–9,13,14} than we consider here. The

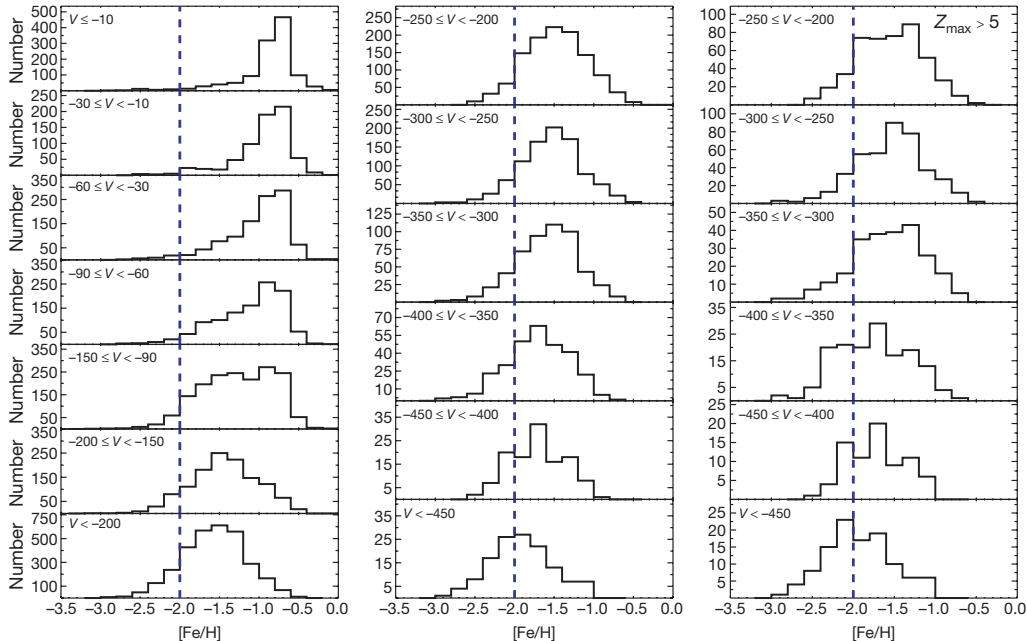


Figure 2 | The distribution of $[\text{Fe}/\text{H}]$ for various cuts in the V velocity (in km s^{-1}), the component of orbital motion measured with respect to the Local Standard of Rest. The Local Standard of Rest is a frame in which the mean space motions of the stars in the solar neighbourhood average to zero. A blue dashed line at $[\text{Fe}/\text{H}] \approx 2.2.0$ is added for reference in all three columns. In the left-hand column, the full data set is considered. The stars with modestly negative V velocities in the upper three panels are dominated by stars from the thick-disk (and metal-weak thick-disk) populations, with a peak metallicity around $[\text{Fe}/\text{H}] \approx 2.0.7$. A transition to dominance by inner- and outer-halo population stars becomes evident for $V \gtrsim 90 \text{ km s}^{-1}$; in the bottom panel of this column, the distribution of $[\text{Fe}/\text{H}]$ appears similar to what in the past was considered ‘the halo’, but we argue results from a

superposition of contributions from both inner- and outer-halo populations. In the middle column, the large numbers of stars with $V \gtrsim 220 \text{ km s}^{-1}$ are broken into smaller ranges in V velocity. As V becomes increasingly retrograde ($V \gtrsim 220 \text{ km s}^{-1}$), the metallicity distribution shifts to include ever larger numbers of stars with $[\text{Fe}/\text{H}] \gtrsim 2.2.0$, and relatively fewer stars with $[\text{Fe}/\text{H}] \approx 2.1.6$. The same V velocity cuts are applied in the right-hand column, but only for stars with $Z_{\text{max}} > 5$ kpc, in order to decrease the contribution from inner-halo stars. Although fewer stars are included, the increasing dominance of stars with $[\text{Fe}/\text{H}] \gtrsim 2.2.0$ is even more apparent. We associate the stars with the most extreme retrograde orbits (and those that reach far above the Galactic plane in their orbits) with the outer-halo population.

stellar samples were obtained with selection criteria (for example, on the basis of high proper motions for halo stars in the solar neighbourhood^{7,13,14}, or from in situ, apparent-magnitude limited surveys^{6,9,15}) that we suggest favoured membership in one or the other of the now clearly revealed halo components. A detailed summary of the kinematics of our programme stars is presented in the Supplementary Information, where we also establish consistency between properties obtained through techniques based on full space motions and those based on radial velocities alone, which argues against the existence of any large systematic errors in the proper motions.

Table 1 summarizes the past and present determinations of \bar{V}_W the mean rotational velocity with respect to the Galactic Centre, where claims for a retrograde halo have been made. Previous samples that have addressed this question were based on either much smaller total numbers of objects (with the limitation that they could not well sample both the inner- and outer-halo populations), did not have proper motions available (or only highly uncertain ones), or were otherwise restricted due to the selection criteria employed (that is, they were kinematically biased¹⁶, or had limited sky coverage, rendering them sensitive to the effects of individual star streams¹⁷). The local sample of SDSS calibration stars we have assembled does not suffer from any of these limitations. The retrograde signatures for stars we associate with the outer-halo population are robust and highly statistically significant (except for the smallest subsample). However, even our precise present determination of the net retrograde rotation of the outer halo, based on our local sample, is probably influenced by some degree of overlap between outer-halo stars with those from the inner-halo population.

The distribution of [Fe/H] for stars on increasingly retrograde orbits about the Galactic Centre for subsamples that reach different distances from the Galactic plane (Z_{\max}) is shown in Fig. 3. The MDFs of the stars with Z_{\max} close to the Galactic plane are very different from those whose orbits reach farther from the plane. The distribution of metallicity clearly shifts to lower abundances as more severe cuts on V_W or Z_{\max} are applied, as supported by rigorous statistical tests. We conclude that the halo of the Galaxy comprises stars with intrinsically different distributions of [Fe/H]; the observed changes in the MDF of halo stars with V_W and Z_{\max} would not be expected if the halo is considered as a single entity. The Supplementary

Information presents additional observed differences in the energetics, the distribution of orbital eccentricities, and changes in the nature of stellar orbits for our programme stars that are also inconsistent with a single halo population.

In order to provide confirmation of the shift in the MDF inferred from our analysis of a local sample of stars, we also examine an auxiliary sample of stars that are at present located much farther from the Galactic Centre. This sample comprises 1,235 blue horizontal-branch stars selected from the SDSS¹⁸. The stars cover a wide range of distances, from 5 kpc to over 80 kpc from the centre of the Galaxy. Statistical tests strongly reject the hypothesis that the stars at large distances from the Galactic Centre could be drawn from the same parent population as those at distances close to the Galactic Centre (Fig. 4).

It has been shown, on the basis of Jeans' theorem^{19,20}, that the global structure of the stellar halo can be recovered from local kinematic information, as long as one has a sufficiently large number of stars observed in the solar neighbourhood that explore the full phase-space distribution of the pertinent stellar populations. We note that the actual halo systems of the Galaxy are unlikely to be in well-mixed equilibrium states. However, the relaxation process is very slow compared to the orbital periods of typical stars, so Jeans' theorem and the approach based on it remain at least approximately valid. The result of this exercise for our large sample of SDSS calibration stars, over narrow cuts in metallicity, is shown in Fig. 5. The observed changes in the inferred spatial density profiles suggest that a flattened inner-halo population dominates locally for stars with [Fe/H] ≥ 2.2 , whereas the outer-halo population has a nearly spherical distribution, and dominates at distances beyond $r \approx 15\text{--}20$ kpc (where r represents the distance from the Galactic Centre), as well as locally for stars with [Fe/H] ≥ 2.0 . Variations in the halo spatial profile with distance have been recognized by a number of previous authors^{1-4,15,20}, based on samples of stars that are one to two orders of magnitude smaller than our present data set.

Implications of the dichotomy of the halo

An early model for the formation of the Milky Way, based on the rapid (a few hundred million years) monolithic collapse of a gaseous proto-Galaxy²¹, has yielded to the more recent idea that the halo of

Table 1 | Studies claiming a retrograde outer halo

Sample and selection criteria	N	Additional restrictions	\bar{V}_W (km s ⁻¹)	Method	Source
Globular clusters (non-kinematic)	19	'Young halo'	264.674	F&W	Ref. 2
Globular clusters (non-kinematic)	20	'Young halo'	242.680	F&W	Ref. 10
RR Lyrae stars (non-kinematic)	26	Z , 8 kpc	295.629	FSM	Ref. 9
Field subdwarfs (kinematic)	30	Z_{\max} , 5 kpc	245.622	FSM	Ref. 7
		Bias corrected	124.613		Ref. 16
Field horizontal-branch stars (non-kinematic)	90	[Fe/H], ≥ 1.6	293.636	F&W	Ref. 8
		Z , 4 kpc			
Field subdwarfs (kinematic)	101	V_W , ≥ 100 km s ⁻¹	232.610	FSM	Ref. 13
		[Fe/H], ≥ 1.8			
Field F, G, K dwarfs (non-kinematic)	250	Z , 5 kpc	255.616	FSM	Ref. 6
Field F, G turnoff (non-kinematic)	2,228	Z_{\max} , 5 kpc	211.62	FSM	This work
	200	[Fe/H], ≥ 1.0	241.611		
		[Fe/H], ≥ 2.2			
	771	Z_{\max} , 10 kpc	238.65		
	94	[Fe/H], ≥ 1.0	271.617		
		[Fe/H], ≥ 2.2			
	371	Z_{\max} , 15 kpc	256.68		
	54	[Fe/H], ≥ 1.0	271.625		
		[Fe/H], ≥ 2.2			

Previous and current determinations of the mean rotational velocity, \bar{V}_W , and the error in the mean (s/\sqrt{N} , where s is the standard deviation and N is the number of stars), for samples in which a counter-rotating halo has been claimed, ordered by sample size. The samples listed in the first column are classified as to whether they were chosen on the basis of high proper motions (kinematic) or not (non-kinematic). Restrictions placed on each sample by the authors are listed in the third column (see original papers for details). The method of analysis used for each determination is listed: F&W, estimate based on the technique of Frenk and White⁴⁸, which considers distances and radial velocities alone, under the assumption of a cylindrically symmetric Galaxy; FSM, estimate based on consideration of the full space motions, which requires the use of proper motions, as well as distances and radial velocities. The samples analysed with the F&W approach are either not statistically different from zero (refs 2, 10), or are only marginally so (2.6s; ref. 8). Previous samples based on analysis of the full space motions vary from statistically insignificant (ref. 7), to just over 3s significance (refs 6, 9, 13), owing to the small numbers of stars considered. Note that after application of (uncertain) corrections for kinematic bias (ref. 16), the retrograde result reported in ref. 7 disappears entirely. One can assume that a similar outcome might apply to the ref. 13 determination. The samples of ref. 6 and ref. 9 are both selected over a restricted region of sky (towards the North Galactic Pole) and are therefore subject to possible contamination by individual stellar streams. All but two subsamples of the SDSS calibration star sample have retrograde signals that are significant at more than the 4s level. The subsample at Z_{\max} , 5 kpc and [Fe/H], ≥ 1 is likely to include significant contamination from inner-halo stars.

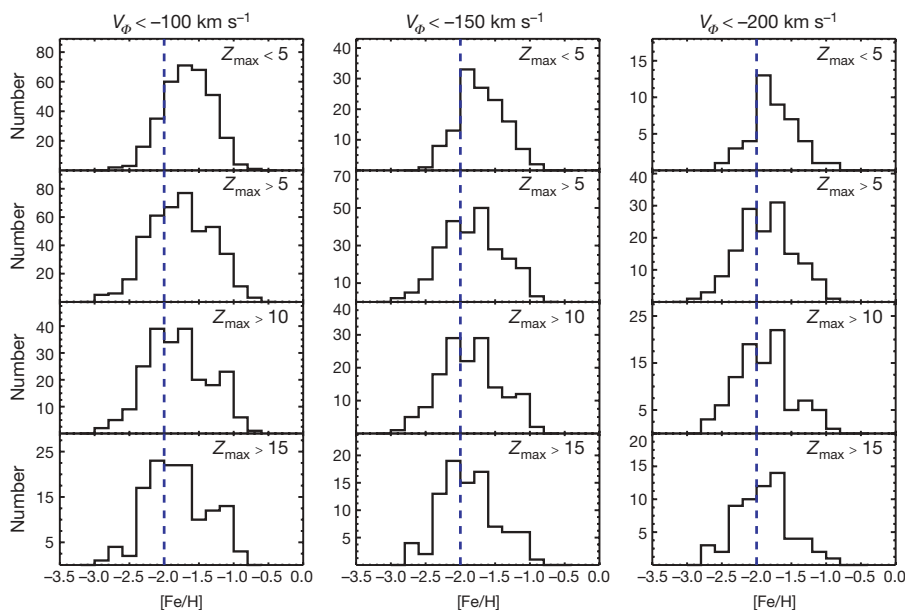


Figure 3 | The distribution of [Fe/H] for the stars in our sample on highly retrograde orbits. Stars from the disk populations, which possess prograde orbits, cannot be present in this plot. The panels show various cuts in V_W , the rotational velocity with respect to the Galactic Centre in a cylindrical coordinate system, and for different ranges of Z_{\max} (in kpc). A blue dashed line at [Fe/H] \approx -2.0 is added for reference. The left-hand column applies for stars with $V_W \gtrsim 100 \text{ km s}^{-21}$; the clearly skewed distribution of [Fe/H] exhibits an increased contribution from lower metallicity stars as one progresses from the low ($Z_{\max} \lesssim 5 \text{ kpc}$) to the high ($Z_{\max} \gtrsim 15 \text{ kpc}$) subsamples. Simultaneously, the predominance of stars from the inner-halo population, with peak metallicity at [Fe/H] \approx -2.1.6, decreases in relative strength, and shifts to lower [Fe/H]. Similar behaviours are seen in the

middle and right-hand columns, which correspond to cuts on $V_W \gtrsim 150 \text{ km s}^{-21}$ and $\gtrsim 200 \text{ km s}^{-21}$, respectively. A Kolmogorov-Smirnoff test of the null hypothesis that the MDFs of stars shown in the lower panels for the individual cuts on V_W could be drawn from the MDFs of the same parent population as those shown in the upper panels, against an alternative that the stars are drawn from more metal-poor parent MDFs, is rejected at high levels of statistical significance. For $V_W \gtrsim 100 \text{ km s}^{-21}$, one-sided probabilities less than 0.0001 are obtained for the cuts on $Z_{\max} \lesssim 5, 10$ and 15 kpc . For $V_W \gtrsim 150 \text{ km s}^{-21}$, one-sided probabilities of 0.0004, 0.0001 and 0.0003 are obtained for $Z_{\max} \lesssim 5, 10$ and 15 kpc , respectively. For $V_W \gtrsim 200 \text{ km s}^{-21}$, one-sided probabilities of 0.014, 0.010 and 0.033 are obtained, for $Z_{\max} \lesssim 5, 10$ and 15 kpc , respectively.

the Galaxy was assembled, over the span of several billion years, from smaller proto-Galactic clumps²². This hierarchical assembly model has received close attention in recent years, in part because it fits well with the prevailing theory for the formation and evolution of structure in the Universe, based on the early collapse of ‘mini-haloes’ of cold dark matter (CDM)^{23,24}. Modern numerical simulations for the

assembly of large spirals based on CDM cosmogonies predict that the stars in the haloes of galaxies like the Milky Way might be composed of the shredded stellar debris of numerous dwarf-like galaxies that have been torn apart by tidal interactions with their parent galaxy^{24–27}. Recent quantitative analysis of the amount of structure visible in the halo of the Galaxy from SDSS^{28–31} imaging provides compelling additional evidence³². Others have argued that some combination of a monolithic collapse and a hierarchical assembly model may be necessary to fully explain the observed data^{2,15,33}.

Within the context of the CDM model, the formation of the inner halo may be understood in the following manner. Low-mass sub-Galactic fragments are formed at an early stage. These fragments

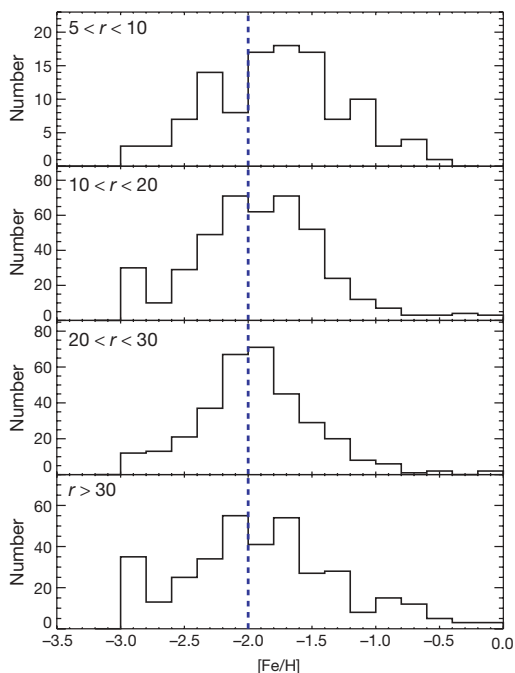


Figure 4 | A sample of blue horizontal-branch stars exploring much larger distances from the Galactic Centre than the SDSS calibration stars. The distribution of [Fe/H] is shown for various cuts on the distance from the Galactic Centre, r , in kpc. The nature of the MDF appears to shift from the upper two panels, which exhibit the character of a mixture of inner- and outer-halo populations, over to a unimodal distribution in the third panel, centred on [Fe/H] \approx -2.2.0. The most distant blue horizontal branch (BHB) stars in the lowest panel also exhibit the appearance of a mixture of the two populations, possibly due to the inclusion of inner-halo stars on highly eccentric orbits that take them far from the Galactic Centre. The peak around [Fe/H] \approx -2.3.0 seen in several of the panels is an artefact arising from the limit of the metallicity grid that is used for abundance determinations of the BHB stars. A Kolmogorov-Smirnoff test of the null hypothesis that the MDFs of stars shown in the lower panels for the individual cuts on Galactocentric distance r could be drawn from the same parent population as the stars shown in the first panel, against an alternative that the stars are drawn from more metal-poor parent MDFs, is rejected at high levels of statistical significance (one-sided probabilities of 0.0262, 0.0005 and 0.0243, respectively, for the three higher cuts on r). The fraction of stars with metallicities [Fe/H] \gtrsim -2.2.0 (primarily outer-halo stars) grows from 31% for stars with $5 < r < 10 \text{ kpc}$ to 46% for stars at larger Galactocentric distances.

rapidly merge into several (in many simulations, two^{26,34}) more-massive clumps, which themselves eventually dissipatively merge (owing to the presence of gas that has yet to form stars). The essentially radial merger of the few resulting massive clumps gives rise to the dominance of the high-eccentricity orbits for stars that we assign here to membership in the inner halo. Star formation within these massive clumps (both pre- and post-merger) would drive the mean metallicity to higher abundances. This is followed by a stage of adiabatic compression (flattening) of the inner halo component owing to the growth of a massive disk, along with the continued accretion of gas onto the Galaxy^{34,35}.

The fact that the outer-halo component of the Milky Way exhibits a net retrograde rotation (and a different distribution of overall orbital properties), as found here, clearly indicates that the formation of the outer halo is distinct from that of both the inner-halo and disk components. We suggest, as others have before, that the outer-halo component formed, not through a dissipative, angular-momentum-conserving contraction, but rather through dissipationless chaotic merging of smaller subsystems within a pre-existing dark-matter halo. These subsystems would be expected to be of much lower mass, and subject to tidal disruption in the outer part of a dark-matter halo, before they fall farther into the inner part. As candidate (surviving) counterparts for such subsystems, one might consider the low-luminosity dwarf spheroidal galaxies surrounding the Galaxy, in particular the most extreme cases recently identified from the SDSS^{36,37}. Subsystems of lower mass, and by inference, even lower metallicity, may indeed be destroyed so effectively that none (or very few) have survived to the present day. If so, the outer-halo population may be assembled from relatively more metal-poor stars, following the luminosity–metallicity relationship for Local Group dwarf galaxies³⁸.

The net retrograde rotation of the outer halo may be understood in the context of the higher efficiency of phase mixing for the orbits of stars that are stripped from subsystems on prograde, rather than retrograde, orbits^{39,40}.

The clear difference in the MDFs of the two halo populations we identify also suggests that the lowest metallicity stars in the Galaxy may be associated with the outer halo, which can be exploited for future directed searches. It is noteworthy that the hyper metal-poor stars HE 010725240⁴¹ and HE 132722326⁴², both of which have $[Fe/H] \approx -2.5$, as well as the recently discovered ultra metal-poor star HE 055724840⁴³, with $[Fe/H] \approx -2.48$, are either located greater than 10 kpc away (HE 010725240, HE 055724840) or have space motions that carry them far out into the Galaxy (HE 132722326; A. Frebel, personal communication).

In addition, efforts to determine the primordial lithium abundance from observations of the most metal-poor stars⁴⁴ may have inadvertently mixed samples from the inner- and outer-halo populations; such stars could have formed and evolved in rather different astrophysical environments. The inner/outer halo dichotomy may also have an impact on the expected numbers of carbon-enhanced metal-poor stars as a function of declining metallicity⁴⁵, and as a function of distance from the Galactic plane^{46,47}.

Much remains to be learned as the database of low-metallicity stars continues to expand, in particular from those stars that are found in distant in situ samples, or from those nearby stars with available proper motions that indicate membership of the outer-halo population. We look forward to the next dramatic increase in the numbers of very metal-poor stars that will come from the ongoing stellar samples from SDSS, and in particular from SEGUE, the Sloan Extension for Galactic Understanding and Exploration.

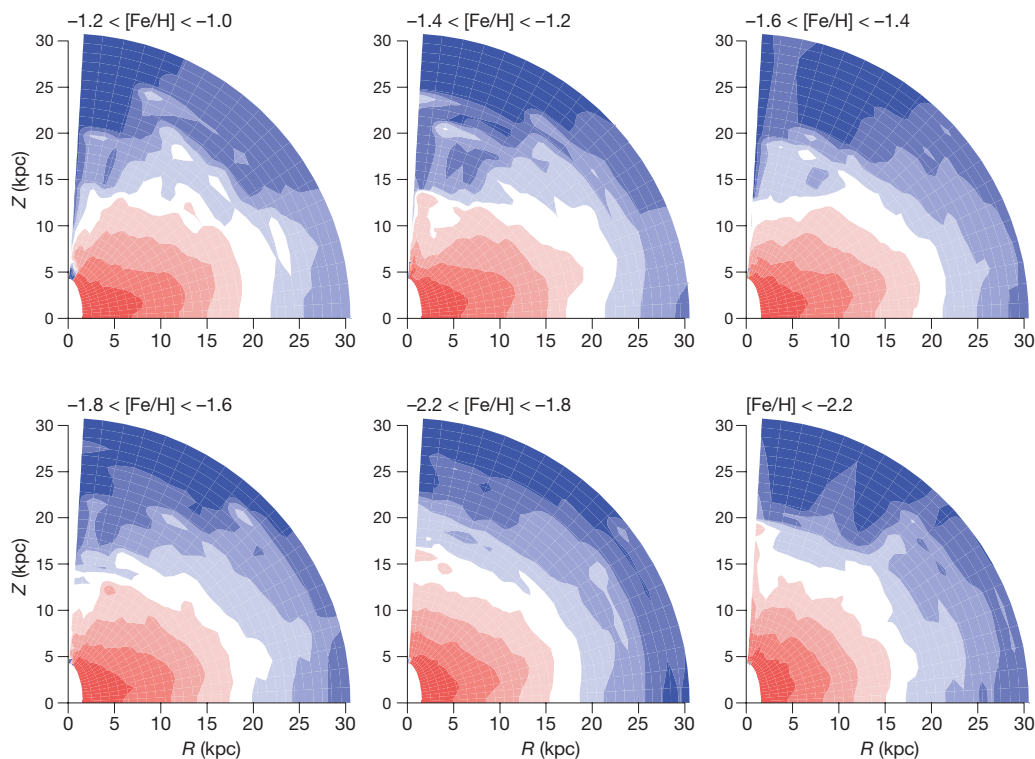


Figure 5 | Equidensity contours of the reconstructed global density distributions for stars in our sample with various metallicities. The global density distributions are constructed from the sum of the probability density of an orbit at each location in the Z – R plane, with a weighting factor being inversely proportional to the corresponding density at the currently observed position of the star^{19,20}. High-density regions are indicated by redder colours, while low-density regions are indicated by bluer colours (a linear density scale is used). Within each metallicity cut, the apparent flattening of the inner regions slowly goes over to a more spherical shape

with increasing distance. As one progresses from the more metal-rich ($[Fe/H] \approx -2.1$) to the most metal-poor ($[Fe/H] \approx -2.2$) subsets of these data, the overall nature of the equidensity contours also changes from highly flattened (axial ratios of ~ 0.6), to more spherical (axial ratio of ~ 0.9). This suggests that the inner- and outer-halo components are broadly overlapping in space and in metallicity—the inner-halo population is characterized as a flattened density distribution that dominates locally for stars with $[Fe/H] \approx -2.2$, whereas the outer-halo population is nearly spherical, and dominates at larger distances and locally for stars with $[Fe/H] \approx -2.2$.

Received 20 June; accepted 5 November 2007.

1. Hartwick, F. D. A. in *The Galaxy* (eds Gilmore, G. & Carswell, B.) 281–290 (NATO ASI Series 207, Reidel, Dordrecht, 1987).
2. Zinn, R. in *The Globular Clusters-Galaxy Connection* (eds Smith, G. H. & Brodie, J. P.) 38–47 (ASP Conf. Ser. 48, Astronomical Society of the Pacific, San Francisco, 1993).
3. Preston, G. W., Shectman, S. A. & Beers, T. C. Detection of a galactic color gradient for blue horizontal-branch stars of the halo field and implications for the halo age and density distributions. *Astrophys. J.* 375, 121–147 (1991).
4. Kinman, T. D., Suntzeff, N. B. & Kraft, R. P. The structure of the galactic halo outside the solar circle as traced by the blue horizontal branch stars. *Astron. J.* 108, 1722–1772 (1994).
5. Miceli, A. et al. Evidence for distinct components of the Galactic stellar halo from 838 RR Lyrae stars discovered in the LONEOS-I survey. *Astrophys. J.* (in the press); preprint at <http://arxiv.org/abs/0706.1583> (2007).
6. Majewski, S. R. A complete, multicolor survey of absolute proper motions to B of about 22.5 – Galactic structure and kinematics at the north Galactic pole. *Astrophys. J.* 78 (Suppl.), 87–152 (1992).
7. Carney, B. W., Laird, J. B., Latham, D. W. & Aguilar, L. A. A survey of proper motion stars. XIII. The halo population(s). *Astron. J.* 112, 668–692 (1996).
8. Wilhelm, R. et al. in *Formation of the Galactic Halo... Inside and Out* (eds Morrison, H. & Sarajedini, A.) 171–174 (ASP Conf. Ser. 92, Astronomical Society of the Pacific, San Francisco, 1996).
9. Kinman, T. D., Cacciari, C., Bragaglia, A., Buzzoni, A. & Spagna, A. Kinematic structure in the Galactic halo at the north Galactic pole: RR Lyrae and BHB stars show different kinematics. *Mon. Not. R. Astron. Soc.* 371, 1381–1398 (2007).
10. Lee, Y.-W., Hansung, B. G. & Casetti-Dinescu, D. I. Kinematic decoupling of globular clusters with extended horizontal branches. *Astrophys. J.* 661, L49–L52 (2007).
11. York, D. G. et al. The Sloan Digital Sky Survey: Technical summary. *Astron. J.* 120, 1579–1587 (2000).
12. Adelman-McCarthy, J. K. et al. The fifth data release of the Sloan Digital Sky Survey. *Astrophys. J.*, Suppl. 172, 634–644 (2007).
13. Sandage, A. & Fouts, G. New subdwarfs. VI. Kinematics of 1125 high-proper-motion stars and the collapse of the Galaxy. *Astron. J.* 92, 74–115 (1987).
14. Ryan, S. G. & Norris, J. E. Subdwarf studies. II – Abundances and kinematics from medium-resolution spectra. III. – The halo metallicity distribution. *Astron. J.* 101, 1835–1864 (1991).
15. Chiba, M. & Beers, T. C. Kinematics of metal-poor stars in the Galaxy. III. Formation of the stellar halo and thick disk as revealed from a large sample of non-kinematically selected stars. *Astron. J.* 119, 2843–2865 (2000).
16. Carney, B. W. in *The Third Stromlo Symposium: The Galactic Halo* (eds Gibson, B. K., Axelrod, T. S. & Putman, M. E.) 230–242 (ASP Conf. Ser. 165, Astronomical Society of the Pacific, San Francisco, 1999).
17. Majewski, S. R., Munn, J. A. & Hawley, S. L. Absolute proper motions to B approximately 22.5: Evidence for kinematical substructure in halo field stars. *Astrophys. J.* 427, L37–L41 (1994).
18. Sirko, E. et al. Blue horizontal-branch stars in the Sloan Digital Sky Survey. I. Sample selection and structure in the Galactic halo. *Astron. J.* 127, 899–913 (2004).
19. Binney, J. & May, A. The spheroids of galaxies before and after disc formation. *Mon. Not. R. Astron. Soc.* 218, 743–760 (1986).
20. Sommer-Larsen, J. & Zhen, C. Armchair cartography – A map of the Galactic halo based on observations of local, metal-poor stars. *Mon. Not. R. Astron. Soc.* 242, 10–24 (1990).
21. Eggen, O. J., Lynden-Bell, D. & Sandage, A. R. Evidence from the motions of old stars that the galaxy collapsed. *Astrophys. J.* 136, 748–766 (1962).
22. Searle, L. & Zinn, R. Compositions of halo clusters and the formation of the galactic halo. *Astrophys. J.* 225, 357–379 (1978).
23. White, S. D. M. & Rees, M. J. Core condensation in heavy halos – A two-stage theory for galaxy formation and clustering. *Mon. Not. R. Astron. Soc.* 183, 341–358 (1978).
24. Moore, B., Diemand, J., Madau, P., Zemp, M. & Stadel, J. Globular clusters, satellite galaxies and stellar haloes from early dark matter peaks. *Mon. Not. R. Astron. Soc.* 368, 563–570 (2006).
25. Bullock, J. S. & Johnston, K. V. Tracing galaxy formation with stellar halos. I. Methods. *Astrophys. J.* 635, 931–949 (2005).
26. Abadi, M. G., Navarro, J. F. & Steinmetz, M. Stars beyond galaxies: The origin of extended luminous haloes around galaxies. *Mon. Not. R. Astron. Soc.* 365, 747–758 (2006).
27. Brook, C. B., Kawata, D., Martel, H., Gibson, B. K. & Scannapieco, E. Chemical and dynamical properties of the stellar halo. *EAS Publ. Ser.* 24, 269–275 (2007).
28. Fukigita, M. et al. The Sloan Digital Sky Survey photometric system. *Astron. J.* 111, 1748–1756 (1996).
29. Gunn, J. E. et al. The Sloan Digital Sky Survey photometric camera. *Astron. J.* 116, 3040–3081 (1998).
30. Pier, J. R. et al. Astrometric calibration of the Sloan Digital Sky Survey. *Astron. J.* 125, 1559–1579 (2003).
31. Gunn, J. E. et al. The 2.5 m telescope of the Sloan Digital Sky Survey. *Astron. J.* 131, 2332–2359 (2006).
32. Bell, E. F. et al. The accretion origin of the Milky Way's stellar halo. *Astrophys. J.* (in the press); preprint at <http://arxiv.org/abs/0706.0004> (2007).
33. Majewski, S. R. Galactic structure surveys and the evolution of the Milky Way. *Annu. Rev. Astron. Astrophys.* 31, 575–638 (1993).
34. Bekki, K. & Chiba, M. Formation of the galactic stellar halo. I. Structure and kinematics. *Astrophys. J.* 558, 666–686 (2001).
35. Chiba, M. & Beers, T. C. Structure of the galactic stellar halo prior to disk formation. *Astrophys. J.* 549, 325–336 (2001).
36. Belokurov, V. et al. The field of streams: Sagittarius and its siblings. *Astrophys. J.* 642, L137–L140 (2006).
37. Belokurov, V. et al. Cats and dogs, hair and a hero: A quintet of new Milky Way companions. *Astrophys. J.* 654, 897–906 (2007).
38. Dekel, A. & Woo, J. Feedback and the fundamental line of low-luminosity low-surface-brightness/dwarf galaxies. *Mon. Not. R. Astron. Soc.* 344, 1131–1144 (2003).
39. Quinn, P. J. & Goodman, J. Sinking satellites of spiral systems. *Astrophys. J.* 309, 472–495 (1986).
40. Norris, J. E. & Ryan, S. G. Population studies: Evidence for accretion of the galactic halo. *Astrophys. J.* 336, L17–L19 (1989).
41. Christlieb, N. et al. A stellar relic from the early Galaxy. *Nature* 419, 904–906 (2002).
42. Frebel, A. et al. Nucleosynthetic signatures of the first stars. *Nature* 434, 871–873 (2005).
43. Norris, J. E. et al. HE 0557–4840 – ultra metal-poor and carbon-rich. *Astrophys. J.* 670, 774–788 (2007).
44. Bonifacio, P. et al. First stars VII. Lithium in extremely metal-poor dwarfs. *Astron. Astrophys. J.* 462, 851–864 (2007).
45. Lucatello, S. et al. The frequency of carbon-enhanced metal-poor stars in the Galaxy from the HERES sample. *Astrophys. J.* 653, L37–L40 (2006).
46. Frebel, A. et al. Bright metal-poor stars from the Hamburg/ESO Survey. I. Selection and follow-up observations from 329 fields. *Astrophys. J.* 652, 1585–1683 (2006).
47. Tumlinson, J. Carbon-enhanced metal-poor stars, the cosmic microwave background, and the stellar IMF in the early universe. *Astrophys. J.* (submitted).
48. Frenk, C. S. & White, S. D. M. The kinematics and dynamics of the galactic globular cluster system. *Mon. Not. R. Astron. Soc.* 193, 295–311 (1980).

Supplementary Information is linked to the online version of the paper at www.nature.com/nature.

Acknowledgements We thank C. Allende Preto, E. Bell, W. Brown, A. Frebel, B. Gibson, H. Morrison, C. Thom, J. Tumlinson and B. Yanny for comments on previous versions of this Article. D.C. acknowledges partial support for travel and living expenses from JINA, the Joint Institute for Nuclear Astrophysics, while in residence at Michigan State University. Funding for the SDSS and SDSS-II has been provided by the Alfred P. Sloan Foundation, the Participating Institutions, the National Science Foundation, the US Department of Energy, the National Aeronautics and Space Administration, the Japanese Monbukagakusho, the Max Planck Society, and the Higher Education Funding Council for England. The SDSS website is <http://www.sdss.org>.

Author Information Reprints and permissions information is available at www.nature.com/reprints. Correspondence and requests for materials should be addressed to D.C. (carollo@mso.anu.edu.au).

